Received: 12 March 2019 | Revised: 11 June 2019 | Accepted: 13 June 2019

DOI: 10.1002/aoc.5097

FULL PAPER

WILEY Applied Organometallic Chemistry

One-pot green synthesis of Cu/bone nanocomposite and its catalytic activity in the synthesis of 1-substituted 1*H*-1,2,3,4-tetrazoles and reduction of hazardous pollutants

Mehdi Maham[1] | **Mahmoud Nasrollahzadeh**[2]

[1]Department of Chemistry, Aliabad Katoul Branch, Islamic Azad University, Aliabad Katoul, Iran

[2]Department of Chemistry, Faculty of Science, University of Qom, Qom 3716146611, Iran

Correspondence
Mehdi Maham, Department of Chemistry, Aliabad Katoul Branch, Islamic Azad University, Aliabad Katoul, Iran.
Email: mehdimaham@gmail.com

Funding information
Iran National Science Foundation (INSF), Grant/Award Number: 96002276

In this work, a simple and green method is reported for the biosynthesis of Cu/bone nanocomposite using *Cordyline fruticosa* extract as a stabilizer and reductant. Animal bone was used as a natural support to prevent the accumulation of Cu nanoparticles. The catalytic activity of Cu/bone nanocomposite was assessed in the synthesis of 1-substituted 1*H*-1,2,3,4-tetrazoles and reduction of various organic dyes, including 4-nitrophenol (4-NP), nigrosin (NS), congo red (CR) and methylene blue (MB). The best catalytic performance in the synthesis of 1-substituted tetrazoles was achieved using 0.05 g of Cu/bone nanocomposite at 120°C. In addition, under optimal conditions, the absorption bands corresponding to 4-NP, CR, NS and MB completely disappeared after about 6 min, 3 min, 50 s and 7 s, respectively. The biosynthesis protocol used in the preparation of Cu/bone nanocomposite offers a very attractive area for further research.

KEYWORDS
1-substituted 1*H*-1,2,3,4-tetrazoles, Cu/bone nanocomposite, green synthesis, hazardous pollutants, natural support

1 | INTRODUCTION

The increase of environmental contaminations caused by pesticides, heavy metals, organic dyes and wastes in water sources calls for the development of basic and applied research concerning environmental protection.[1] Nitroarene compounds and toxic dyes are considered important pollutants in wastewaters due to their stability in the environment.[2] Chemical coagulation, microbiological discoloration and physical adsorption are traditional methods to treat wastewater containing synthetic dye molecules.[3–5] However, these common techniques have several limitations, and there are still challenges to develop effective methods to convert the pollutants in wastewater to non-toxic products.

Tetrazoles have many applications in pharmaceuticals, photography, information recording systems and rocket propellants, and function as isosteric substituents for analytical reagents and carboxylic acids.[6,7] In general, these heterocycles are synthesized by the cycloaddition of trimethyl azide/hydrazoic acid and isocyanides,[8,9] and cyclization of ammonium salts with hydrazoic acid metal salts or ortho carboxylic esters.[10,11] 1-substituted 1*H*-1,2,3,4-tetrazoles are important ligands due to their biological activity.[12] However, their widespread use requires easy and effective synthesis methods.

Nanomaterials and nanocomposites have distinctive and interesting properties for application in different industrial fields.[13–19] Synthesis of Cu nanoparticles (NPs) has attracted considerable attention owing to the availability and low price of copper.[18,19] However, in most cases, Cu NPs are unstable under reaction conditions, and have a tendency for aggregation causing the loss of their unique properties. A stabilizer purpose is used to avoid agglomeration and control the size of the particles. Different types of solid wastes such as bones, eggshells and mollusk shells can be used as supports to produce low-cost catalysts.[20–22] In this sense, animal bone is regarded as one of the best solid wastes, which is abundant and easily available throughout the world. The inorganic composition of bone is composed of hydroxyapatite (HAP).[23,24] HAP is a stable phosphate mineral with high adsorption capacity. The structures of pure and bone HAP are extremely similar, but there exist small differences owing to the presence of ions such as iron in the bone HAP structure.

Various techniques and methods, including sonochemical route,[25] sol–gel,[26] hydrothermal approach,[27] chemical bath deposition,[28] chemical reduction,[29] microwave irradiation[30] and thermal decomposition[31] are used to synthesize nanomaterials. These methods require high pressure and temperature, toxic reagents, and a number of dangerous chemicals are absorbed on the surface of NPs, which may cause adverse effects especially in medical applications. Therefore, the search for the synthesis method of NPs using a green and convenient method under mild conditions is imperative.

The biosynthesis of NPs has attracted particular attention owing to its inherent characteristics, including use of natural products, lack of toxicity, rapidness, and providing conditions to synthesize controlled and well-defined size of NPs.[32–37] These interesting features are necessary for medical applications.

The genus *Cordyline* distributed in the Southern hemisphere is widely found in Australia and New Zealand. *Cordyline fruticosa*, which belongs to the family of *Asparagaceae*, is a woody plant. The different parts of *C. fruticosa* have been traditionally used for the treatment of various diseases, such as treatment of hemostatic, toothache, laryngitis, bloody cough, dysentery, fever, headache, inflammation of the digestive tract, kidney diseases and blood in urine (Figure 1). Reports published on *C. fruticosa* indicate a rich phytochemical content mainly consisting of flavonoids, glycosides, alkaloids, saponins, phenolics and tannins. The water extract of the plant exclusively contains flavonoids and phenolic glycosides with considerable antioxidant power.[38–40] The present study reports the preparation of Cu/bone nanocomposite using *C. fruticosa* extract, its catalytic activity as a heterogeneous catalyst in the synthesis of 1-substituted 1*H*-1,2,3,4-tetrazoles under solvent-free and thermal conditions, and reduction of various organic dyes such as 4-nitrophenol (4-NP), nigrosine (NS), congo red (CR) and methylene blue (MB) using $NaBH_4$ in water at ambient temperature.

FIGURE 1 Image of *Cordyline fruticosa* plant

2 | RESULTS AND DISCUSSION

2.1 | Green synthesis and characterization of Cu/bone nanocomposite

Cu/bone nanocomposite was synthesized through a green method using *C. fruticosa* aqueous extract as a reductant and stabilizer agent. The characterization of *C. fruticosa* aqueous extract was performed using UV–Vis spectroscopy. Figure 2 shows the UV absorption bands at

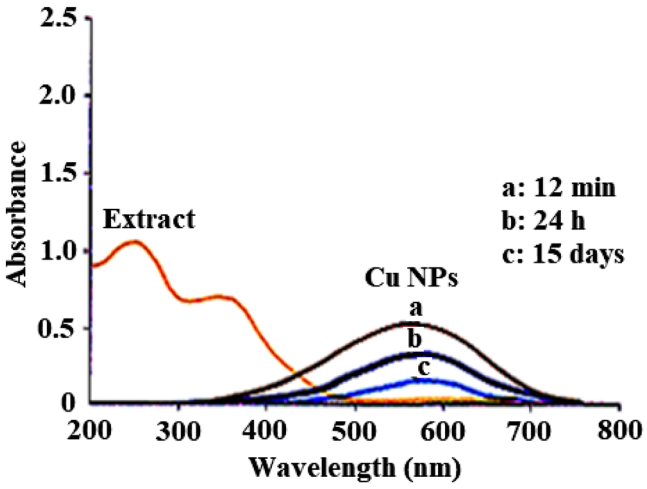

FIGURE 2 UV–Vis spectra of *Cordyline fruticosa* extract and biosynthesized Cu nanoparticles (NPs)

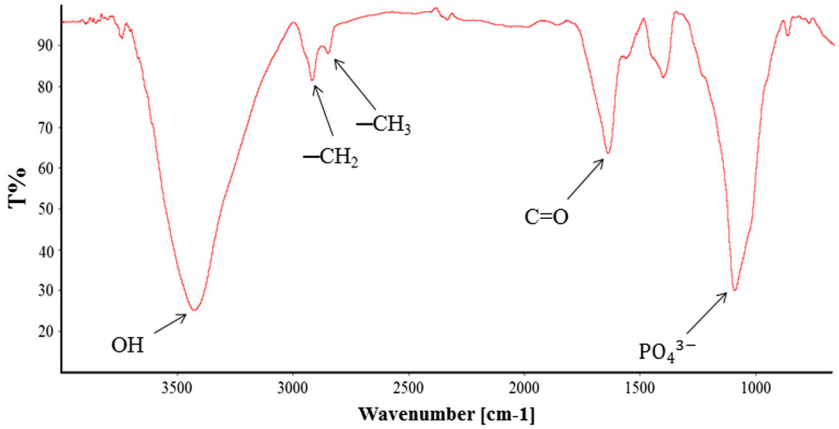

FIGURE 3 Fourier transform-infrared (FT-IR) spectrum of bone powder

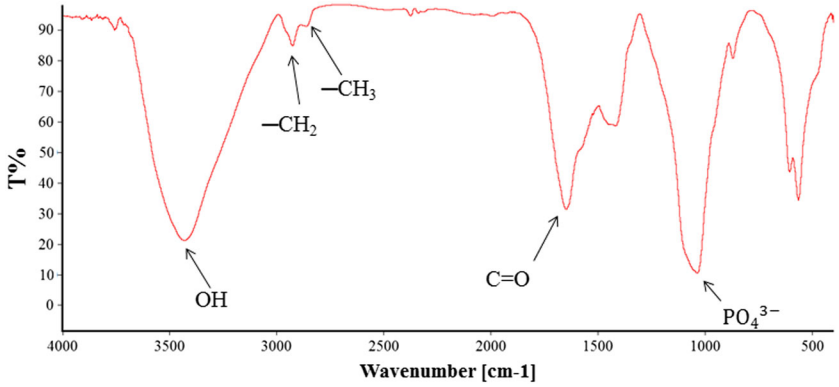

FIGURE 4 Fourier transform-infrared (FT-IR) spectrum of Cu/bone nanocomposite

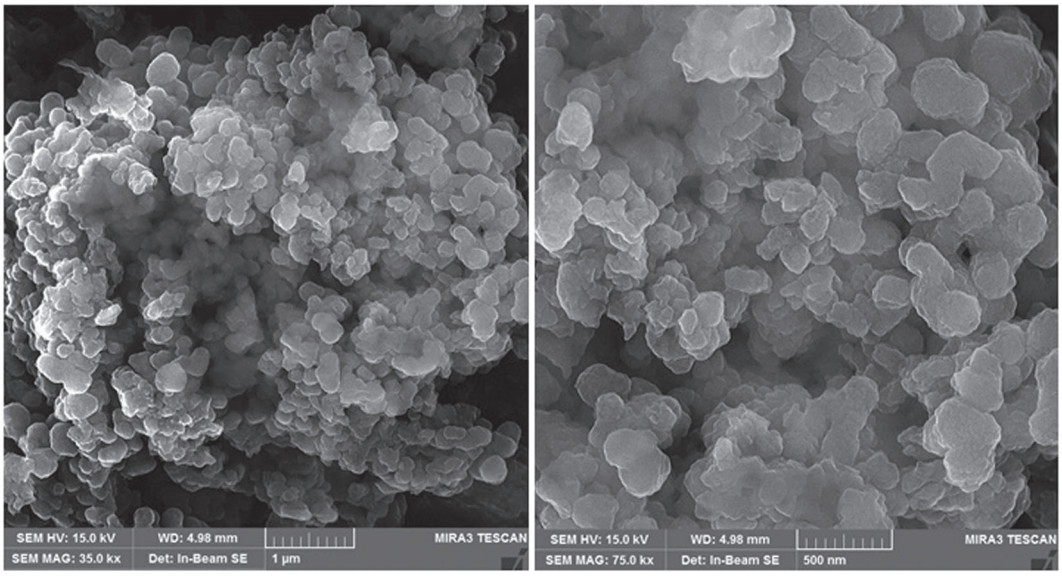

FIGURE 5 Field emission-scanning electron microscopy (FE-SEM) images of Cu/bone nanocomposite

350 nm (band I) and 250 nm (band II) associated with the cinnamoyl and benzoyl systems, respectively. These absorption bands reveal the presence of phenolics as antioxidant sources for the green synthesis of Cu NPs. The UV–Vis spectrum corresponding to the biosynthesized Cu NPs shows the surface plasmon

resonance signal following the change of the solution color, which verifies the successful synthesis of Cu NPs.

The Fourier transform-infrared (FT-IR) spectrum of bone (Figure 3) shows a signal at about 3436 cm^{-1}, which is attributed to the stretching vibration of hydrogen-bonded hydroxyl groups. The C-H stretching bands at 2925 (asymmetric) and 2864 cm^{-1} (symmetric) correspond to $-CH_2$ and $-CH_3$ groups, respectively.[41] Furthermore, the peaks at about 1645 and 1098 cm^{-1} are assigned to the stretching vibrations of amides and PO_4^{3-} groups, respectively.[41] As expected, due to the similarity of the functional groups in bone and Cu/bone nanocomposite, almost the same pattern is observed in the FT-IR spectrum of Cu/bone nanocomposite (Figure 4), where the signals at about 3433, 2962, 2865, 1649 and 1035 cm^{-1} are attributed to the stretching vibrations of hydrogen-bonded hydroxyl groups, $-CH_2$ and $-CH_3$ groups, and stretching vibrations of amides and PO_4^{3-} groups, respectively.

To study the morphology of the biosynthesized Cu/bone nanocomposite, field emission-scanning electron microscopy (FE-SEM) analysis was performed. As is shown in Figure 5, Cu grain has permeated into the bone surface, resulting in the perfect integration between bone and Cu NPs.

The X-ray diffraction (XRD) analysis of the bone powder shows crystalline phase of $Ca_{10}(PO4)_6(OH)_2$ (JCPDS No.:74–0566).[42] The XRD pattern corresponding to the Cu/bone nanocomposite is shown in Figure 6. The broad peak at $2\theta = 31.8^{o}$ is attributed to the characteristic peak of HAP, which indicates its amorphous nature. No characteristic peaks are observed for Cu in the pattern of Cu/bone nanocomposite, indicating that the Cu NPs are highly dispersed on the bone support or the reflection

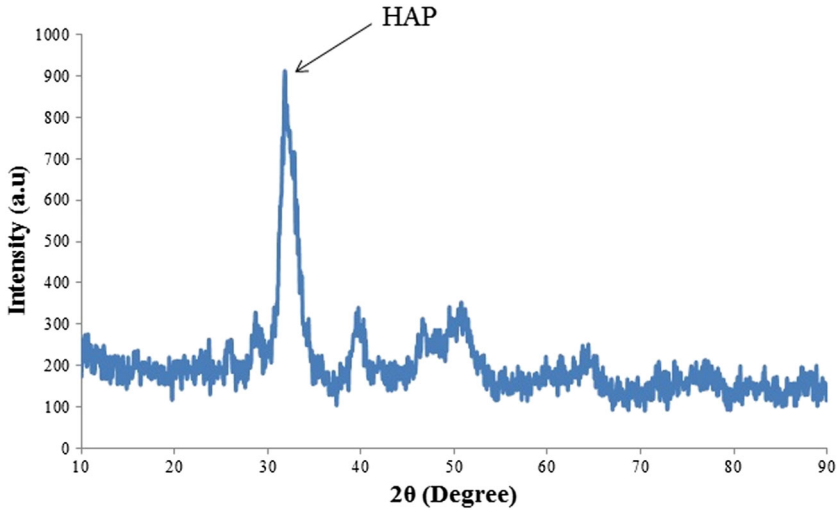

FIGURE 6 X-ray diffraction (XRD) pattern of Cu/bone nanocomposite

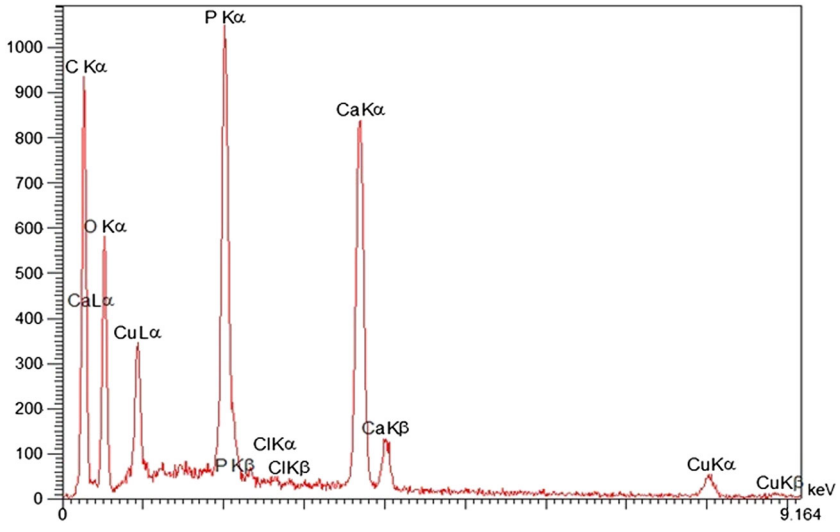

FIGURE 7 Energy-dispersive X-ray spectroscopy (EDS) spectrum of Cu/bone nanocomposite

peaks of the bone with high intensity overlap with Cu NPs peaks.

To confirm the presence of metallic Cu in the as-synthesized nanocomposite and investigate the constituent elements of the Cu/bone nanocomposite, energy-dispersive X-ray spectroscopy (EDS) analysis was performed, and the results are presented in Figure 7. The presence of the Cu, Ca, O, Cl, P and C peaks in the EDS spectrum confirms the formation of the Cu/bone nanocomposite. Moreover, the EDS elemental mapping of Cu/bone nanocomposite is shown in Figure 8. Obviously, the presence of Cu, Ca, O, Cl, P and C has been established using elemental mapping.

The transmission electron microscopy (TEM) analysis was performed to obtain extra information about the Cu/bone nanocomposite morphology (Figure 9).

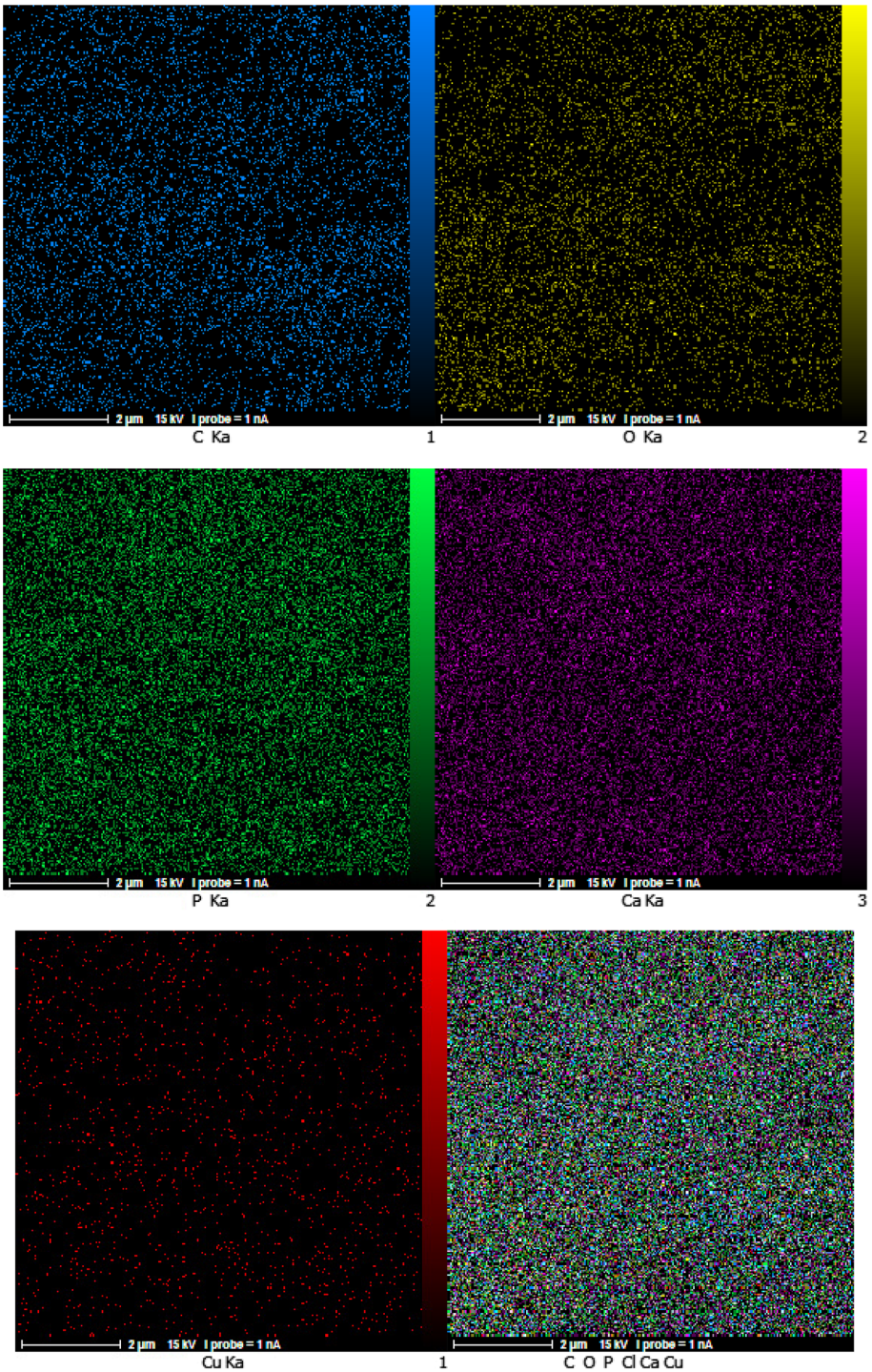

FIGURE 8 Elemental mapping of Cu/bone nanocomposite

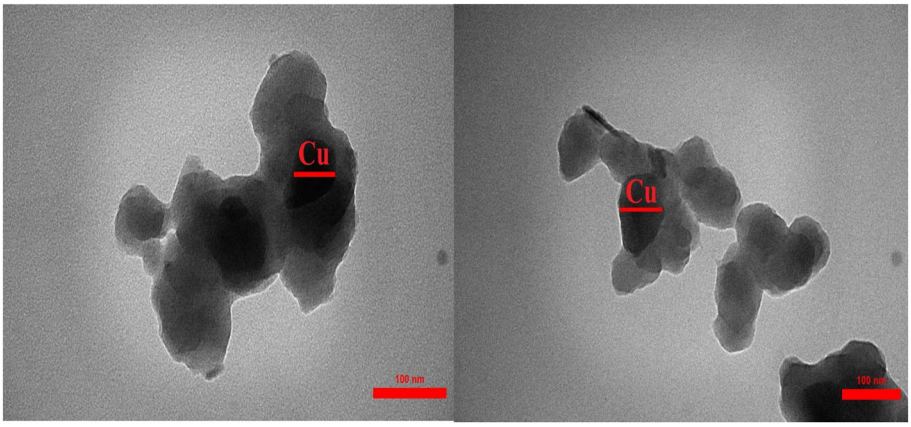

FIGURE 9 Transmission electron microscopy (TEM) images of Cu/bone nanocomposite

According to the size distribution histogram, the average size of Cu NPs on the surface of bone support is about 45 nm (Figure 10).

Polyphenolic compounds present in the *C. fruticosa* leaf extract are likely to facilitate the formation of nano zero-valent copper. The possible bio-reduction mechanism is proposed as follows:

$$nFIOH + M^{+n} \rightarrow nFIO\ (radical) + nM^0$$

$$nFIO\ (radical) + M^{n+} \rightarrow nFIOX + nM^0 (Nucleation)$$

$$nM^0 + Mn^+ \rightarrow M_n^{n+} (Growth)$$

$$M_n^{n+} + M_n^{n+} \rightarrow M_{2n}^{2n+}$$

$$\left(M_{2n}^{2n+}\right)_n + (FIOH)_n \rightarrow \text{metallic NZV}$$

where FlOH and NZV are polyphenolic (flavonoids) and nano zero-valent, respectively.

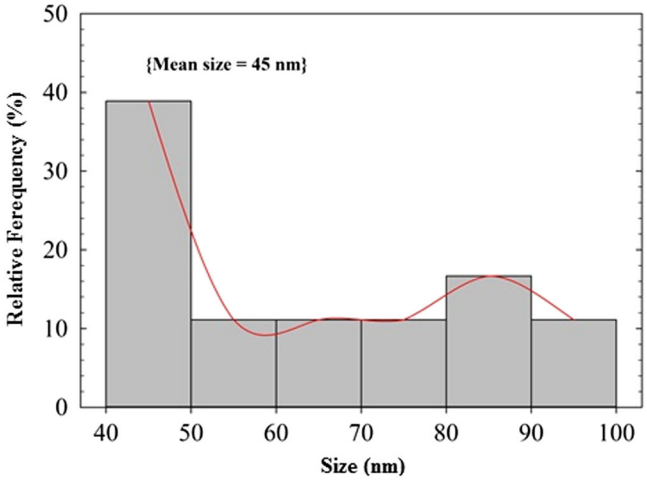

FIGURE 10 Cu nanoparticles (NPs) size distributions

2.2 | The catalytic performance of Cu/bone nanocomposite in the synthesis of 1-substituted 1*H*-1,2,3,4-tetrazoles

In order to evaluate the catalytic activity of the as-prepared nanocomposite, 1-substituted tetrazoles were synthesized using a wide variety of primary amines,

TABLE 1 The effect of temperature and catalyst loading in the synthesis of 1-(4-chlorophenyl)-1*H*-1,2,3,4-tetrazole[a]

Entry	Catalyst (g)	Temperature/°C	Time (hr)	Yield[b] (%)
1	0.0	120	4	0.0
2	0.03	90	4	61
3	0.03	120	4	81
4	0.05	120	3	93
5	0.05	100	4	79
6	0.07	120	3	93

[a]Reaction conditions: 2.0 equiv. of 4-chloroaniline, 2.4 equiv. of $CH(OEt)_3$, 2.0 equiv. of NaN_3.

[b]Isolated yield.

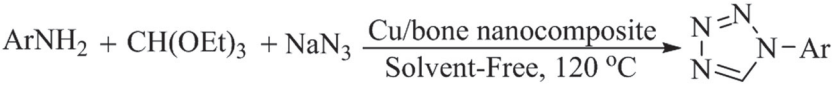

SCHEME 1 Synthesis of 1-substituted 1*H*-1,2,3,4-tetrazoles

TABLE 2 Synthesis of 1-substituted 1*H*-1,2,3,4-tetrazoles using Cu/bone nanocomposite at 120°C[a]

Entry	Amine	Product	Yield[b] (%)
1	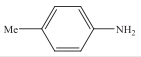	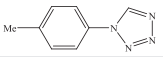	92
	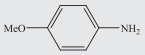	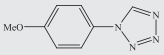	93
2		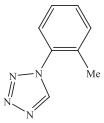	91
3	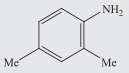	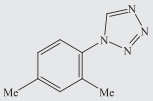	84
	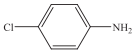	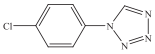	93
4		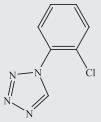	83
5	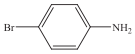	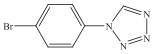	90
6	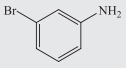	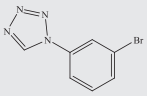	89
7	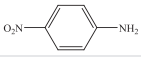	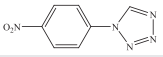	83
8		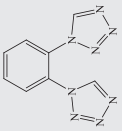	85

[a]Reaction conditions: amine (2.0 mmol), 2.4 equiv. of $CH(OEt)_3$, 2.0 equiv. of NaN_3, catalyst (0.05 g), 120°C, 3 hr.

[b]Yields are after work-up.

triethyl orthoformate, sodium azide and Cu/bone nanocomposite as catalyst under solvent-free conditions. Initial studies were carried out to optimize the reaction conditions for the synthesis of 1-(4-chlorophenyl)-1*H*-1,2,3,4-tetrazole (Scheme 1). As predicted, no reaction occurs in the absence of Cu/bone nanocomposite even after 4 hr (Table 1, entry 1). The best result was achieved using 0.05 g of Cu/bone nanocomposite at 120°C (Table 1, entry 4). Increasing the catalyst loading to more than 0.05 g did not significantly improve the performance (Table 1, entry 6).

In addition, a variety of primary aromatic amines possessing both electron-withdrawing and -donating groups were converted into the corresponding 1-substituted 1*H*-1,2,3,4-tetrazoles (Table 2). Based on the results, amines with different substituents in *ortho*, *meta* or *para* positions were efficiently converted to the corresponding 1-substituted tetrazoles in good to excellent yields.

The as-synthesized Cu/bone nanocomposite probably acts as a Lewis acid in the promotion of the cyclization process (Scheme 2). According to the plausible mechanism, the elimination of EtOH and consequently the formation of 1-substituted 1*H*-1,2,3,4-tetrazole is catalyzed by the breakdown of the C-OEt bond in triethyl orthoformate in the presence of the catalyst.

2.3 | The catalytic performance of Cu/bone nanocomposite in the reduction of 4-NP, NS, MB and CR

In this study, the catalytic activity of Cu/bone nanocomposite was investigated via the reduction of 4-NP to 4-aminophenol (4-AP) in the presence of $NaBH_4$. 4-NP

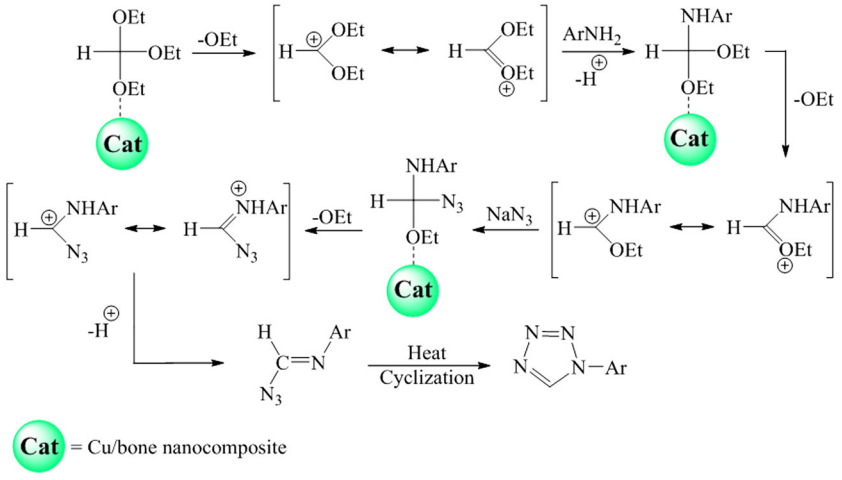

SCHEME 2 Plausible mechanism for the formation of 1-substituted 1*H*-1,2,3,4-tetrazoles

solution shows a λ_{max} of 317 nm (Figure 11). The solution color changes to dark yellow immediately after the addition of $NaBH_4$ to the 4-NP solution due to the formation of 4-nitrophenolate ions. The λ_{max} observed at 400 nm confirms the formation of 4-nitrophenolate ions. In the absence of the nanocatalyst, the λ_{max} at 400 nm remains constant during 100 min (Table 3, entry 1). After adding the as-prepared Cu/bone nanocatalyst, the λ_{max} of 4-nitrophenolate decreased and a new peak appeared at 297 nm due to the formation of 4-AP. The effects of different concentrations of nanocatalyst and $NaBH_4$ on the catalytic reduction of 4-NP were assessed, and optimal results were obtained using 10.0 mg of the nanocatalyst and 100 equivalents of $NaBH_4$ (Table 3, entry 4). Furthermore, the catalytic activity of Cu/bone nanocomposite was compared with that of the unmodified bone, and the results are shown in Table 3, entry 8. The lower catalytic performance of bone in comparison with Cu/bone nanocomposite is attributed to the main role of Cu NPs in the catalyst structure. A possible mechanism for catalysis in the 4-NP reduction reaction by Cu/bone nanocomposite is presented in Scheme 3. At first, metal hydride is formed by the adsorption of $NaBH_4$ onto the surface of the catalyst. 4-NP is then adsorbed onto the surface of the catalyst, and electron transfer mediated by metal surfaces from BH_4^- to 4-NP occurs. Finally, the desorption of the desired analyte causes free space to continue the reaction.

The catalytic performance of Cu/bone nanocomposite in the reduction of 4-NP is compared with that of the

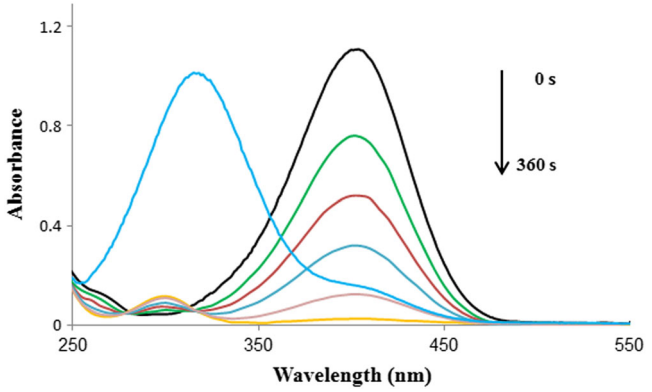

FIGURE 11 UV–Vis spectra of 4-nitrophenol (4-NP) aqueous solution in the presence of 100 equivalents of $NaBH_4$ and 10.0 mg of the Cu/bone nanocatalyst

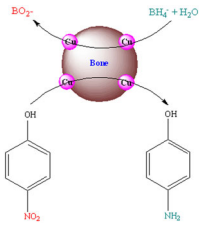

SCHEME 3 Mechanism of reduction of 4-nitrophenol (4-NP) to 4-aminophenol (4-AP) in the presence of Cu/bone nanocatalyst and $NaBH_4$

TABLE 3 Effect of the Cu/bone nanocatalyst loading and concentration of $NaBH_4$ in the reduction of 4-NP (2.5×10^{-3} M) to 4-AP

Entry	Nanocatalyst (mg)	$NaBH_4$ (equivalents)	Time
1	-	100	100 min[a]
2	Cu/bone nanocomposite (5.0)	100	13 min
3	Cu/bone nanocomposite (7.0)	100	8 min
4	Cu/bone nanocomposite (10.0)	100	6 min
5	Cu/bone nanocomposite (10.0)	79	17 min
6	Cu/bone nanocomposite (10.0)	50	24 min
8	Bone (10.0)	100	40 min[a]

[a]No reaction.

TABLE 4 Comparison of the catalytic performance for the reduction of 4-NP to 4-AP over various catalysts

Entry	Catalyst	Time	Reference
1	Micron-SiO_2@nano-Ag	12 min	[43]
2	Pd/FG[a]	12 min	[44]
3	Ag-Fe_3O_4@chitin	10 min	[45]
4	HMMS-NH_2-Pd[b]	60 min	[46]
5	Ag/TiO_2-Cu	25 min	[47]
6	PtNPs AmLig[c]	180 min	[48]
7	PdCu/graphene	1.5 hr	[49]
8	XG/Ag NPs[d]	24 hr	[50]
9	Cu NPs	50 min	[51]
10	Cu/bone	6 min	This work

[a]FG, functionalized graphene.

[b]HMMS, hollow magnetic mesoporous spheres.

[c]AmLig, ammonium derivatives of the lignin samples.

[d]XG, xanthan gum.

TABLE 5 Effect of the catalyst loading in the reduction of CR, NS and MB

Entry	Dye (M)	$NaBH_4$ (M)	Catalyst (mg)	Time
1	CR (1.44×10^{-5})	5.3×10^{-3}	Bone (5.0)	1 hr[a]
2	CR (1.44×10^{-5})	5.3×10^{-3}	Bone (10.0)	1 hr[a]
3	CR (1.44×10^{-5})	5.3×10^{-3}	Cu/bone nanocomposite (5.0)	4 min
4	CR (1.44×10^{-5})	5.3×10^{-3}	Cu/bone nanocomposite (7.0)	3 min
5	CR (1.44×10^{-5})	5.3×10^{-3}	Cu/bone nanocomposite (10.0)	3 min
6	NS (1.62×10^{-4})	5.3×10^{-3}	Bone (10.0)	40 min[a]
7	NS (1.62×10^{-4})	5.3×10^{-3}	Cu/bone nanocomposite (5.0)	130 s
8	NS (1.62×10^{-4})	5.3×10^{-3}	Cu/bone nanocomposite (7.0)	80 s
9	NS (1.62×10^{-4})	5.3×10^{-3}	Cu/bone nanocomposite (10.0)	50 s
10	MB (3.1×10^{-5})	5.3×10^{-3}	Bone (10.0)	40 min[a]
11	MB (3.1×10^{-5})	5.3×10^{-3}	Cu/bone nanocomposite (5.0)	12 s
12	MB (3.1×10^{-5})	5.3×10^{-3}	Cu/bone nanocomposite (7.0)	7 s

[a]No reaction.

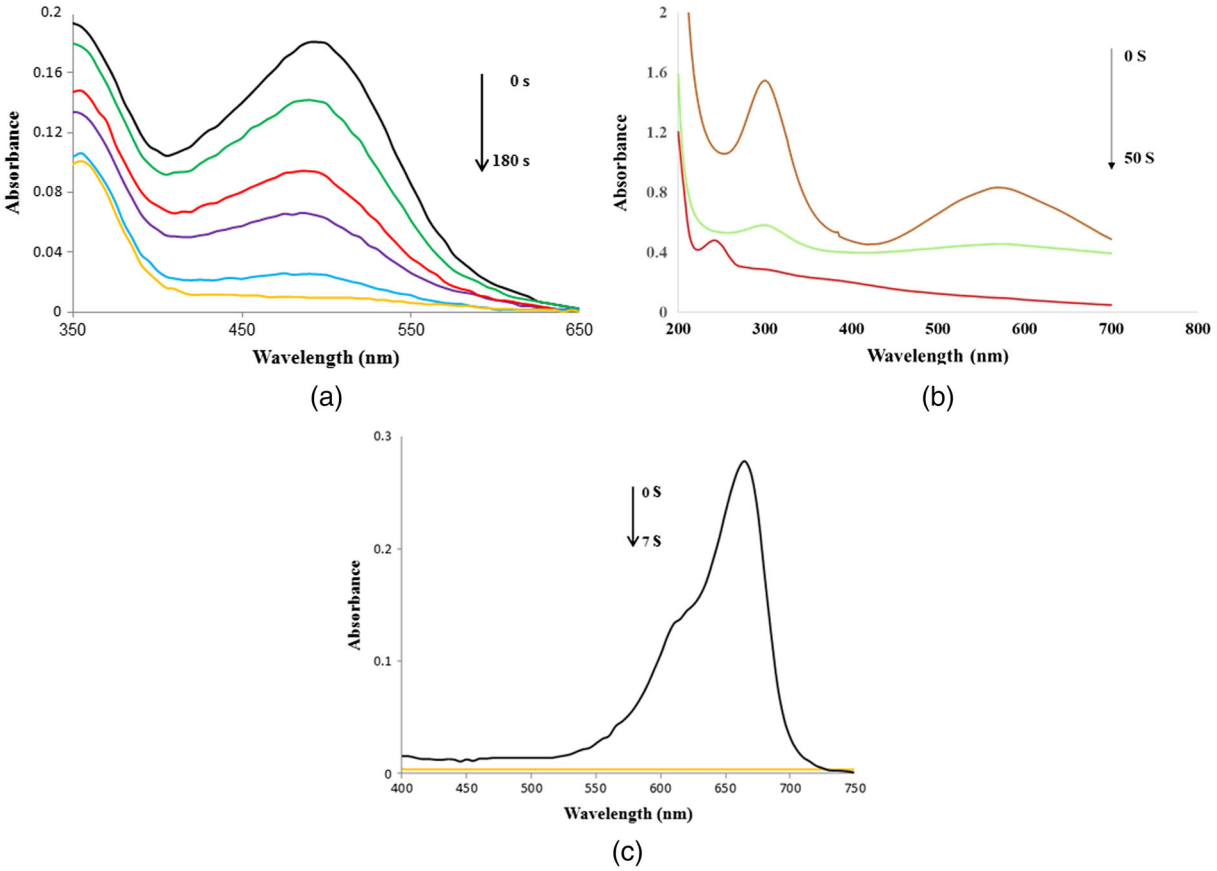

FIGURE 12 UV–Vis absorption spectra of reduction of (a) congo red (CR), (b) nigrosine (NS) and (c) methylene blue (MB) aqueous solution by Cu/bone nanocatalyst under the optimal conditions

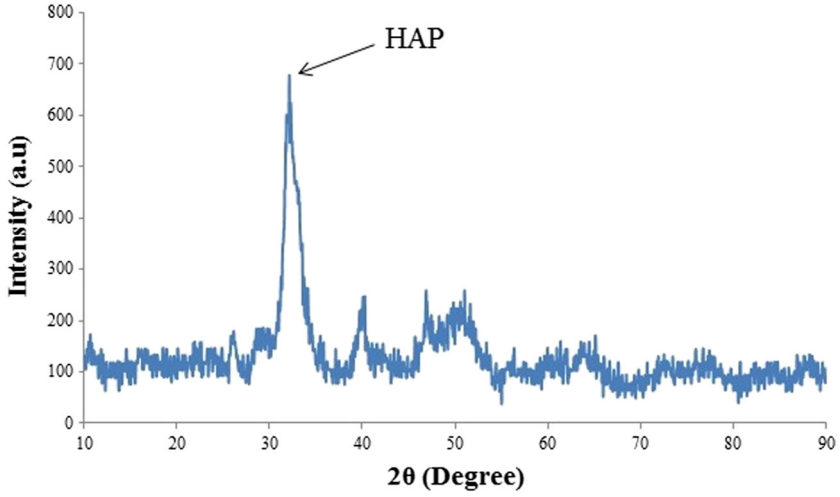

FIGURE 13 X-ray diffraction (XRD) pattern of recycled Cu/bone nanocomposite

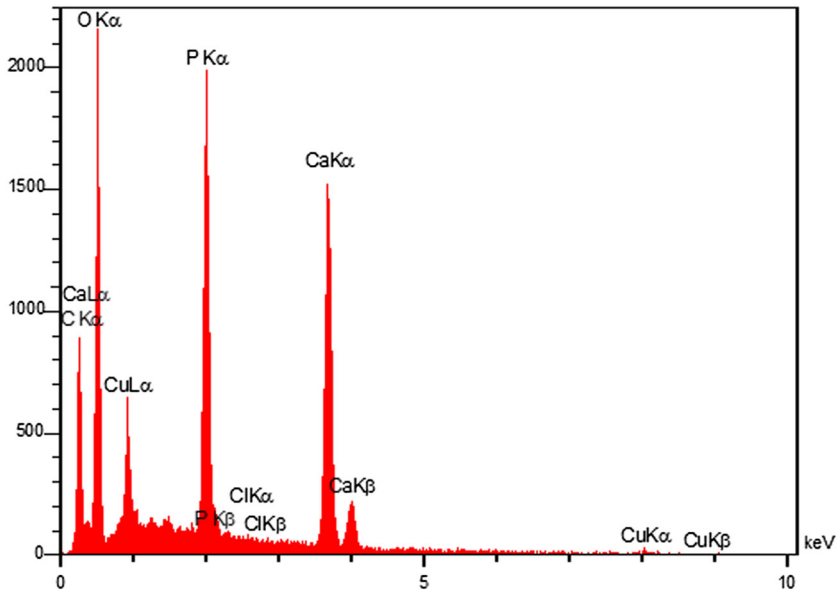

FIGURE 14 Energy-dispersive X-ray spectroscopy (EDS) spectrum of recycled Cu/bone nanocomposite

other catalysts reported in the papers, and the results indicate that the current nanocomposite possesses higher catalytic activity compared with other catalysts (Table 4).

Moreover, the catalytic activity of Cu/bone nanocomposite was investigated in the reduction of NS, MB and CR in the presence of $NaBH_4$ (5.3×10^{-3} M) as the hydrogen source, and the results are presented in Table 5. As predicted, unmodified bone shows a lower catalytic activity in the desired analytes. Under the optimal conditions, the λ_{max} corresponding to CR, NS and MB completely disappeared within 3 min, 50 s and 7 s, respectively (Figure 12).

2.4 | Catalyst recyclability

The recyclability of the biosynthesized nanocomposite was investigated in the synthesis of 1-phenyl-1*H*-1,2,3,4-tetrazole and reduction of organic dyes. At the end of the reaction, the as-synthesized nanocatalyst was separated from the reaction mixture by centrifugation. The separated catalyst was washed with ethanol, deionized water, dried, and reused in another run. The XRD image of Cu/bone nanocomposite exhibits no remarkable change in the morphology, shape and size after four runs (Figure 13). This was further confirmed by EDS analysis and elemental mapping of the recycled catalyst (Figures 14 and 15).

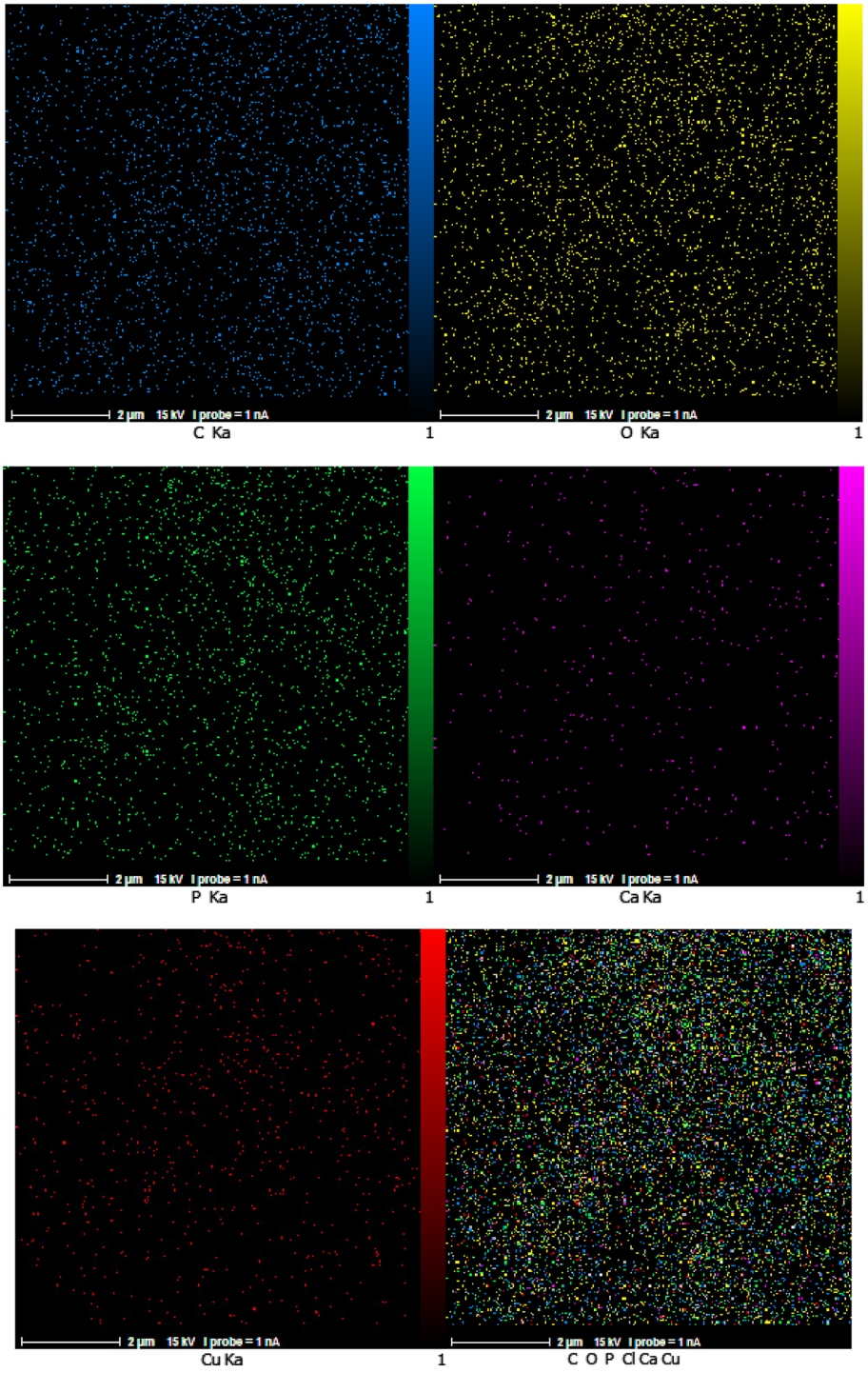

FIGURE 15 Elemental mapping of recycled Cu/bone nanocomposite

3 | CONCLUSION

In conclusion, a green, simple, sustainable and low-cost method has been reported for the synthesis of Cu/bone nanocomposite. The application of the *C. fruticosa* extract as reducing and stabilizing agent efficiently removed toxic and hazardous chemicals. In addition, using bone, a natural support, prevents the aggregation of Cu NPs, controls the size of NPs and, as a result, considerably affects the performance of the biosynthesized nanocomposite. Cu/bone nanocomposite was applied as a heterogeneous catalyst in the synthesis of 1-substituted 1*H*-1,2,3,4-tetrazoles and reduction of several organic dyes, including 4-NP, NS, MB and CR. According to the results obtained, 1-substituted 1*H*-1,2,3,4-tetrazoles were prepared in high yields using biosynthesized nanocomposite

via an inexpensive and simple methodology. In addition, the as-synthesized nanocatalyst was more efficient in the reduction of desired analytes compared with other catalysts reported in the literature.

4 | EXPERIMENTAL

4.1 | Instruments and materials

All commercially materials were of analytical grade, and were purchased from Merck and Aldrich. FT-IR analysis was carried out by a Nicolet 370 FT/IR spectrophotometer (Thermo Nicolet, USA). XRD analysis was performed using a Philips powder diffractometer model PW 1373 goniometer with monochromatic Cu Kα radiation ($\lambda = 1.5406$) at the speed of 2°/min in the 2θ between 10° and 90°. UV–Vis experiments were carried out using a Hitachi, U-2900 double-beam spectrophotometer. FE-SEM images were recorded using Cam scan MV2300 FE–SEM to evaluate the morphology of the as-synthesized naocomposites. The biosynthesized Cu/bone nanocomposite chemical composition was investigated using EDS, carried out in FE-SEM. TEM analysis was performed by a Philips EM208 microscope with an accelerating voltage of 90 kV.

4.2 | Preparation of *Cordyline fruticosa* extract

Dried powder of the *C. fruticosa* leaves (50 g) was poured into 500 ml of distilled water at 80°C over 30 min. After filtration of the resulting aqueous extract, it was kept at 4°C prior to the next use.

4.3 | Green synthesis of Cu NPs

In order to synthesize Cu NPs, 50 ml of the plant extract was mixed with 50 ml of 0.005 M $CuCl_2{\cdot}2H_2O$ solution with constant stirring at 80°C until the color of the mixture changed, indicating the formation of the target product. Reducing Cu^{2+} to Cu^0 was finished in 12 min (as checked with UV–Vis spectra). The Cu NPs biosynthesized using *C. fruticosa* extract were quite stable for a period of 15 days, as shown in Figure 2.

4.4 | Preparation of bone

Chicken leg bone, which has large amounts of carbonated HAP, was used as the support in the preparation of the nanocomposite. Chicken bone was thoroughly washed with cold water, and its bone marrow was removed, dried, powdered and finally rinsed with boiling ethanol.

4.5 | Biosynthesis of Cu/bone nanocomposite

To prepare Cu/bone nanocomposite, 50 ml of the aqueous extract of *C. fruticosa* was added to a dispersion containing 25 ml of a $CuCl_2{\cdot}2H_2O$ solution (0.005 M) and 1.0 g of bone. The mixture obtained was then agitated for 4 hr at 80°C. The precipitate formed after cooling the solution was filtered, rinsed with distilled water and finally dried in an oven at 120°C for 5 hr.

4.6 | General procedure for the synthesis of 1-substituted 1*H*-1,2,3,4-tetrazoles

A mixture of the as-synthesized Cu/bone nanocomposite (0.05 g), NaN_3 (2.0 mmol), amine (2.0 mmol) and triethyl orthoformate (2.4 mmol) was heated and stirred at 120°C for 3 hr. Upon completion of the reaction, as confirmed by thin-layer chromatography, the reaction mixture was diluted and extracted with cold water (5 ml) and ethyl acetate (3 × 10 ml), respectively. Afterwards, the catalyst was filtered, and the combined organic layers were washed with brine and dried using anhydrous $MgSO_4$. The pure compounds were obtained after concentration and a crystallizaton step using EtOAc–hexane solvent mixture. All tetrazoles were known compounds and characterized by melting points or spectral analysis.[52–54]

4.7 | Reduction of 4-NP by Cu/bone nanocomposite

In general, 10.0 mg of the Cu/bone nanocomposite and 25 ml of 2.5 mM aqueous solution of 4-NP were transferred into a beaker, and the mixture obtained was agitated for 2 min. Next, 25 ml of freshly prepared $NaBH_4$ aqueous solution (5.3×10^{-3} M) was added, and the reduction procedure was controlled through decreasing λ_{max} 400 nm with UV–Vis absorption spectroscopy. Finally, the nanocatalyst was recovered and reused in the next reaction.

4.8 | Reduction of NS, MB and CR by Cu/bone nanocomposite

Normally, excess $NaBH_4$ (25 ml, 5.3×10^{-3} M) was added to the beaker containing 10.0 mg of the Cu/bone nanocomposite and 25 ml of NS aqueous solution (1.62×10^{-4} M). The changes in the absorption band at

580 nm were recorded simultaneously until the solution became colorless. Moreover, similar procedures were used to assess the catalytic performance of the as-synthesized nanocomposite in the reduction of MB and CR. In each reaction, the amounts of $NaBH_4$ and nanocatalyst added were 5.3×10^{-3} M and 7.0 mg, respectively. In addition, the concentrations of MB and CR aqueous solutions were 3.1×10^{-5} and 1.44×10^{-5} M, respectively. The reaction completion was established with the change of the λ_{max} values of 663 and 493 nm for MB and CR, respectively.

ACKNOWLEDGEMENTS

The authors gratefully thank the Iran National Science Foundation (INSF) for supporting this project numbered 96002276. The authors also gratefully acknowledge the Islamic Azad University, Aliabad Katoul branch for the support of this work.

ORCID

Mehdi Maham https://orcid.org/0000-0002-5438-333X
Mahmoud Nasrollahzadeh https://orcid.org/0000-0002-4539-3544

REFERENCES

[1] J. C. Spain, *Annu. Rev. Microbiol.* **1995**, *49*, 523.
[2] W. Zhang, X. Xiao, T. An, Z. Song, J. Fu, G. Sheng, M. Cui, *J. Chem. Technol. Biotechnol.* **2015**, *78*, 788.
[3] F. El-Gohary, A. Tawfik, *Desalination* **2009**, *249*, 1159.
[4] F. J. Cervantes, A. B. D. Santos, *Rev. Environ. Sci. Bio.* **2011**, *10*, 125.
[5] L. Lucarelli, V. Nadtochenko, J. Kiwi, *Langmuir* **2000**, *16*, 1102.
[6] A. R. Katritzky, B. V. Rogovoyand, K. V. Kovalenko, *J. Org. Chem.* **2003**, *68*, 4941.
[7] M. L. Kantam, K. B. S. Kumar, K. P. Raja, *J. Mol. Catal. A Chem.* **2006**, *247*, 186.
[8] M. P. Taterao, A. S. Shafi, J. L. Rajgopal, V. S. Kumar, *Tetrahedron Lett.* **2007**, *48*, 1721.
[9] T. Jin, S. Kamijo, Y. Yamamoto, *Tetrahedron Lett.* **2004**, *45*, 435.
[10] Y. Satoh, N. Marcopulos, *Tetrahedron Lett.* **1995**, *36*, 1759.
[11] A. K. Gupta, C. H. Oh, *Tetrahedron Lett.* **2004**, *45*, 4113.
[12] H. Shahroosvand, L. Najafi, E. Mohajerani, A. Janghouri, M. Nasrollahzadeh, *RSC Adv.* **2013**, *3*, 6323.
[13] G. Sharma, D. D. Dionysiou, S. Sharma, A. Kumar, A. H. Al-Muhtaseb, M. Naushad, F. J. Stadler, *Catal. Today* **2019**, *335*, 437. https://doi.org/10.1016/j.cattod.2019.03.063
[14] B. Thakur, M. Naushad, A. H. Al-Muhtaseb, A. Kumar, M. Sillanpaa, G. T. Mola, *Mater. Chem. Phys.* **2017**, *193*, 129.
[15] M. Thakur, G. Sharma, T. Ahamad, A. A. Ghfar, D. Pathania, M. Naushad, *Colloids Surf. B. Biointerfaces* **2017**, *157*, 456.
[16] G. Sharma, A. Kumar, M. Naushad, A. Kumar, A. H. Al-Muhtaseb, P. Dhiman, A. A. Ghfar, F. J. Stadler, M. R. Khan, *J. Clean. Prod.* **2018**, *172*, 2919.
[17] G. Sharma, S. Bhogal, M. Naushad, A. Kumar, F. J. Stadler, *J. Photochem. Photobiol.* **2017**, *347*, 235.
[18] P. Zhang, T. Song, T. Wang, H. Zeng, *Appl. Catal. B* **2017**, *206*, 328.
[19] U. Rasool, S. Hemalatha, *Mater. Lett.* **2017**, *194*, 176.
[20] M. Nasrollahzadeh, S. M. Sajadi, A. Hatamifard, *Appl. Catal. Environ.* **2016**, *191*, 209.
[21] Y. Li, Y. Jiang, J. Gao, *Energ. Source Part A* **2015**, *37*, 598.
[22] R. Chakraborty, S. Bepari, A. Banerjee, *Chem. Eng. J.* **2010**, *165*, 798.
[23] R. Chakraborty, D. RoyChowdhury, *Chem. Eng. J.* **2013**, *215–216*, 491.
[24] R. Chakraborty, P. Mukhopadhyay, B. Kumar, *Energ. Conver. Manage.* **2016**, *126*, 32.
[25] H. Yu, H. Fan, X. Wang, J. Wang, P. Cheng, *Optik-Int. J. Light Electron Optics* **2015**, *126*, 4397.
[26] T. Pandiyarajan, R. Udayabhaskar, S. Vignesh, R. A. James, B. Karthikeyan, *Mater. Sci. Eng. C* **2013**, *33*, 2020.
[27] P. Bhavani, C. H. Rajababu, M. D. Arif, I. V. S. Reddy, N. R. Reddy, *J. Magn. Magn. Mater.* **2017**, *426*, 459.
[28] M. M. Momeni, Z. Nazari, *Ceram. Int.* **2016**, *42*, 8691.
[29] Y. Luo, L. A. Estudillo-Wong, N. Alonso-Vante, *Int. J. Hydrogen Energy* **2016**, *41*, 19 601.
[30] J. He, L. Zhou, J. Liu, L. Yang, L. Zou, J. Xiang, S. Dong, X. Yang, *Appl. Surf. Sci.* **2017**, *402*, 469.
[31] T. Kavitha, S. Haider, T. Kamal, M. Ul-Islam, *J. Alloys Compd* **2017**, *704*, 296.
[32] M. Ismail, S. Gul, M. I. Khan, M. A. Khan, A. M. Asiri, S. B. Khan, *Green Process. Synth.* **2019**, *8*, 135.
[33] M. Gangarapu, S. Sarangapany, D. P. Suja, V. B. R. Arava, *Appl. Nanosci.* **2018**, *8*, 1123.
[34] M. Maham, R. Karami-Osboo, *Iran J. Pharm. Res.* **2017**, *16*, 462.
[35] P. Vishnukumar, S. Vivekanandhan, S. Muthuramkumar, *Appl. Organomet. Chem.* **2017**, *4*, 18.
[36] M. Maham, M. Nasrollahzadeh, M. Bagherzadeh, M. R. Akbari, *Comb. Chem. High Throughput Screen.* **2017**, *20*, 787.
[37] M. Maham, M. Nasrollahzadeh, S. M. Sajadi, M. Nekoei, *J. Colloid Interface Sci.* **2017**, *497*, 33.
[38] R. T. Fouedjou, R. T. Fouedjou, E. P. Nguelefack-Mbuyo, B. K. Ponou, T. B. Nguelefack, L. Barboni, L. A. Tapondjou, *Pharmacol. Ther.* **2016**, *7*, 103.
[39] G. Blunden, J. A. Jaffer, K. Jewers, W. J. Griffin, *J. Nat. Prod.* **1981**, *44*, 441.
[40] A. A. Dahlia, A. R. Ahmad, M. Wahid, *J. Biol. Sci. Opinion* **2013**, *1*, 294.
[41] J. H. Park, J. S. Cho, Y. S. Ok, S. H. Kim, S. W. Kang, I. W. Choi, J. S. Heo, R. D. DeLaune, D. C. Seo, *J. Environ. Sci. Health* **2015**, *50*, 1194.
[42] K. Fukui, N. Arimitsu, K. Jikihara, T. Yamamoto, H. Yoshida, *J. Hazard. Mater.* **2009**, *168*, 1617.
[43] M. Wang, D. Tian, P. Tian, L. Yuan, *Appl. Surf. Sci.* **2013**, *283*, 389.

[44] W. Dong, S. Cheng, C. Feng, N. Shang, S. Gao, C. Wang, *Cat. Com.* **2017**, *90*, 70.

[45] B. Duan, F. Liu, M. He, L. Zhang, *Green Chem.* **2014**, *16*, 2835.

[46] P. Wang, F. Zhang, Y. Long, M. Xie, R. Li, J. Ma, *Cat. Sci. Technol.* **2013**, *3*, 1618.

[47] A. Hernández-Gordillo, V. R. González, *Chem. Eng. J.* **2015**, *261*, 53.

[48] F. Coccia, L. Tonucci, D. Bosco, M. Bressan, N. d'Alessandro, *Green Chem.* **2012**, *14*, 1073.

[49] A. K. Shil, D. Sharma, N. R. Guha, P. Das, *Tetrahedron Lett.* **2012**, *53*, 4858.

[50] W. Xu, W. Jin, L. Lin, C. Zhang, Z. Li, Y. Li, R. Song, B. Li, *Carbohydr. Polym.* **2014**, *101*, 961.

[51] P. Deka, R. C. Deka, P. Bharali, *New J. Chem.* **2014**, *38*, 1789.

[52] T. Jin, S. Kamijo, Y. Yamamoto, *Tetrahedron Lett.* **2004**, *45*, 9435.

[53] T. M. Potewar, S. A. Siddiqui, R. J. Lahoti, K. V. Srinivasan, *Tetrahedron Lett.* **2007**, *48*, 1721.

[54] D. Habibi, M. Nasrollahzadeh, T. A. Kamali, *Green Chem.* **2011**, *13*(12), 3499.

How to cite this article: Maham M, Nasrollahzadeh M. One-pot green synthesis of Cu/bone nanocomposite and its catalytic activity in the synthesis of 1-substituted 1*H*-1,2,3,4-tetrazoles and reduction of hazardous pollutants. *Appl Organometal Chem*. 2019;e5097. https://doi.org/10.1002/aoc.5097